Substructuring for Contact Parameters Identification in Bladed-disks

Substructuring for Contact Parameters Identification in Bladed-disks

IOP Conf. Series: Journal of Physics: Conf. Series **1264** (2019) 012037 doi:10.1088/1742-6596/1264/1/012037

Substructuring for Contact Parameters Identification in Bladed-disks

Z Saeed, C M Firrone and T M Berruti

Department of Mechanical Engineering, Politecnico di Torino, Corso Duca degli Abruzzi, 24, 10129 Turin, Italy

E-mail: zeeshan.saeed@polito.it

Abstract. Single stage bladed-disks are fundamental bricks of the rotating parts of a turbomachine. Although made of nominally identical sectors, the presence of imperfections or misalignment produces a large amplification of the forced response. Furthermore, due to their high modal density, friction dampers must be designed to mitigate resonance stresses, since a perfect detuning of the resonances from the excitation forces is impossible. Blade-root joints in these structures can provide the much-desired damping but the contact between the disk slot platform and blade-root lobes is characterized by uncertainty due to the actual locking position and machining tolerances.

The cases of two simple beams and a bladed-disk test rig of an array of blades with dovetail root joints are studied to identify contact parameters. A dynamic Lagrange multiplier frequency based sub-structuring (LM-FBS) method is applied in a hybrid manner (experimental and numerical frequency response functions) to identify a parameter associated to each contact by mounting only one blade at a time. A sensitivity analysis is performed that will provide the basis for future work on non-linear frequency response prediction.

1. Introduction

Bladed-disks form an integral part of a turbo-machine that undergo high vibration amplitudes. Even though they can ideally be described by identical sector due to their periodicity [1], yet small geometrical or manufacturing discrepancies can cause high amplification of the vibration amplitudes [2]. Numerous studies in the past have investigated mistuned blade sectors and it has been shown that its effects are detrimental [3, 4] to the component life. In order to curb the high cycle fatigue (HCF) failures in mistuned structures, some solutions pertain to intentional mistuning [5, 6] and other resort to dampening the response. The available sources of damping in the bladed-disks are either aerodynamic, material or contact friction [7]. The first two being very small may usually not be enough. The contacts in a bladed-disk at blade to blade or blade to disk interfaces are useful for damping but the phenomenon is highly non-linear [8, 9, 10]. Due to its displacement dependent behavior, the contact state prediction remains uncertain. On the other hand, contact state in all the joints of the bladed-disks can cause damping variability or in other words, contact friction mistuning, which has also been reported to cause high response amplification [11].

In order to identify the contact parameters in joints, component mode synthesis (CMS) substructuring or Frequency Based Substructuring (FBS) can be done. A thorough review of the substructuring is given in [12]. In the latter methodology, the substructures can be coupled

at the interfaces with a few number of interface degrees of freedom (DoFs) frequency response functions (FRFs) instead of complete modal parameters estimation. By decoupling the interfaces again, if there is any compliance at the interface, the interface flexibility can be determined in terms of stiffness and damping [13]. A full experimental substructuring is quite difficult because of some practical issues such as drive point FRFs [14, 15], measuring correctly the rigid body modes, noise polluted signals, [16]. Several techniques have been suggested, for example, including the rotations by direct measurements [17] or estimating by translational DoFs [18], or by equivalent multi-point connection (EMPC) [19], or by virtual point transformation with rigid and flexible interface modes [20] etc. Some researchers have also used a hybrid approach where one component's experimental FRFs are used and for the other numerical FRFs are used to reconstruct the response of the coupled structure [21]. The hybrid approach can help model relatively complex geometries and interfaces but measurements are needed at one of the substructure's interface which could be a problem due to inaccessibility.

The FBS method based on Lagrange multipliers (LM-FBS) [22] provides a convenient way of coupling the substructures. In this paper, the LM-FBS method, in its classical form, is applied to two different test-cases i.e. a two-beams assembly and a bladed-disk assembly. For the first test-case, each beam's (substructure) FRFs are acquired experimentally and then their numerical models are updated to match the measured FRFs. The FRFs from the models with different interface configurations are reconstructed by LM-FBS and decoupled from the measured FRF of the coupled beams (assembly). In this way, residual interface flexibility is determined in terms of stiffness and damping for the beams assembly. By this approach, the measurements are needed at only accessible DoFs (with a possibility to avoid interface DoFs) for substructure model updating. The learning from this test-case's results are then used to model the second test-case, in which one blade at a time is assembled to the disk for sensitivity analysis of the interface behavior using different parameters. The work is aimed to provide a basis for better understanding of the interface behavior between the blade and the disk and onward non-linear analysis such as proposed recently in [23].

Section 2 presents a brief mathematical background of the LM-FBS and FRF decoupling method. The application of the method in a hybrid way is demonstrated on the test-case of two beams in Section 3 by using different interface DoFs. After drawing some important inferences, the second test-case of a bladed-disk in Section 4 is studied for sensitivity analysis for interface DoFs that can be helpful in the future investigations followed by the conclusions in Section 5.

2. Mathematical Background

This section will cover briefly the theory of Lagrange multiplier based FBS (LM-FBS). The readers can refer to [12] for more details. If a structure can be divided into two or more substructures, each will have an equation of motion in the frequency domain as:

$$(K^{(s)} + i\omega D^{(s)} - \omega^2 M^{(s)})\bar{\mathbf{u}}^{(\mathbf{s})} = \bar{\mathbf{f}}^{(\mathbf{s})} + \bar{\mathbf{g}}^{(\mathbf{s})} \tag{1}$$

$$Z^{(s)} = K^{(s)} + i\omega D^{(s)} - \omega^2 M^{(s)} \tag{2}$$

where $K^{(s)}$, $D^{(s)}$, $M^{(s)}$ are the stiffness, damping and mass matrices, $Z^{(s)}$ is the dynamic stiffness or impedance of each substructure s at frequency ω, the vector $\bar{\mathbf{u}}^{(\mathbf{s})} = \{u_i^{(s)} \quad u_c^{(s)}\}^T$ contains the substructure's internal $u_i^{(s)}$ and boundary or connection $u_c^{(s)}$ DoFs, $\bar{\mathbf{f}}^{(\mathbf{s})}$ the external forces and $\bar{\mathbf{g}}^{(\mathbf{s})}$ the reaction forces at the interface DoFs. The dynamic stiffness of each substructure is assembled in a block diagonal matrix Z, considering only two substructures, for example:

$$Z = \begin{bmatrix} Z^{(1)} & 0 \\ 0 & Z^{(2)} \end{bmatrix} \tag{3}$$

The equations are assembled in a dual way [22] such that the equilibrium is satisfied at the interface DoFs exactly:

$$\begin{aligned} Z\bar{\mathbf{u}} + B^T\lambda &= \bar{\mathbf{f}} \\ B\bar{\mathbf{u}} &= \bar{\mathbf{0}} \end{aligned} \tag{4}$$

where B is a signed Boolean matrix applying the displacement or kinematic compatibility at the interface. Here $\bar{\mathbf{u}}$ and $\bar{\mathbf{f}}$ contain DoFs and external forces on all the substructures. λ is a vector of Lagrange multipliers. Using the flexibility or FRF matrix notation $Y = Z^{-1}$ and solving for the flexibility of the coupled structure, one obtains $Y^{(FBS)}$ such that:

$$Y^{(FBS)} = Y - YB^T(BYB^T)^{-1}BY \tag{5}$$

If the interface behaves rigidly, any decoupling at the interface will result in zero flexibility. However, the structural joints exhibit some flexibility, no matter how tightly joined. By including all the inertial effect in the two substructures, the interface behaviour can be identified in stiffness terms, as shown in [13] with a demonstration in Fig.1. Considering that the coupled structure and the substructure dynamics are known, the interface can be identified by one of the equations of FRF decoupling given in [21]:

$$Z^*_{int} = [\, Y^{(1)}_{ci}.[Y^{(C)}_{oi}]^{-1}.Y^{(2)}_{oc} - Y^{(1)}_{cc} - Y^{(2)}_{cc}\,]^{-1} \tag{6}$$

where the subscript o belongs to internal DoFs of substructure 2 and is used here to indicate the 'output' DoF. The coupled structure's FRF $Y^{(C)}_{oi}$ is obtained either experimentally or numerically. Z^*_{int} is composed of a stiffness k and a damping c term corresponding to respective m^{th} and n^{th} interface DoFs in Eq.7:

$$Z^*_{int} = k_{mn} + i\omega c_{mn} \tag{7}$$

For the second test-case in this study, the finite element model becomes too large for further sensitivity analyses, therefore, a reduced order model is obtained by applying Hurty Craig Bampton reduction [24] and then using the LM-FBS for coupling the substructures. With constraint modes $\Psi^{(s)}$ and a truncated set of fixed interface modes $\Phi^{(s)}$ results in a reduced set of DoFs and by including appropriately, some internal (response DoFs) $u^{(s)}_i$ and all the interface DoFs $u^{(s)}_c$, $\bar{\mathbf{u}}^{(\mathbf{s})}$ becomes

$$\bar{\mathbf{u}}^{(\mathbf{s})} = \begin{Bmatrix} u^{(s)}_i \\ u^{(s)}_c \end{Bmatrix} \approx \begin{bmatrix} \Phi^{(s)} & \Psi^{(s)} \end{bmatrix} \bar{\mathbf{u}}^{(\mathbf{s})}_{\mathbf{red}} = \begin{bmatrix} \phi^{(s)} & \psi^{(s)} \\ 0 & I \end{bmatrix} \begin{Bmatrix} q^{(s)} \\ u^{(s)}_c \end{Bmatrix} \tag{8}$$

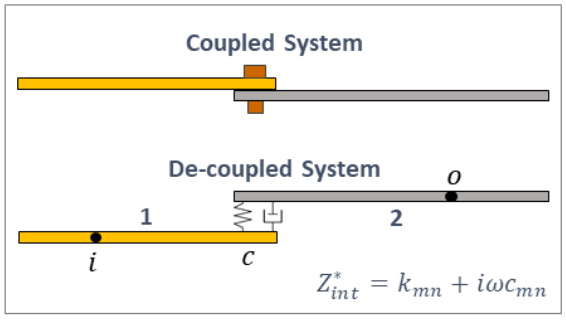

Figure 1. A simple demonstration of decoupling a coupled structure and substructures at the interface.

3. Test-Case 1 - Two Cantilevered Beams

The outlined theory is applied to a case of two cantilevered beams of Aluminum as substructures and joined at their free-ends when assembled, as shown in Fig.2. The excitation and response points are marked as i on beam-1 and o on beam-2 and the interface points as a and b. The FRFs are obtained experimentally using impact hammer at the points labelled as 'excitation' in the figure and the response is measured at the points labelled as 'response' on the individual beams and the assembly. The response measurement is performed by Laser Doppler Vibrometer (LDV) measuring only the out-of-plane deflections. The measured FRFs are plotted in Fig.3(a) and (b) as black dashed lines. The main resonance peaks correspond to the bending modes. It is worth-mentioning that the bolts for joining are considered as part of beam-1 and kept tightened on it during measurements acquisition.

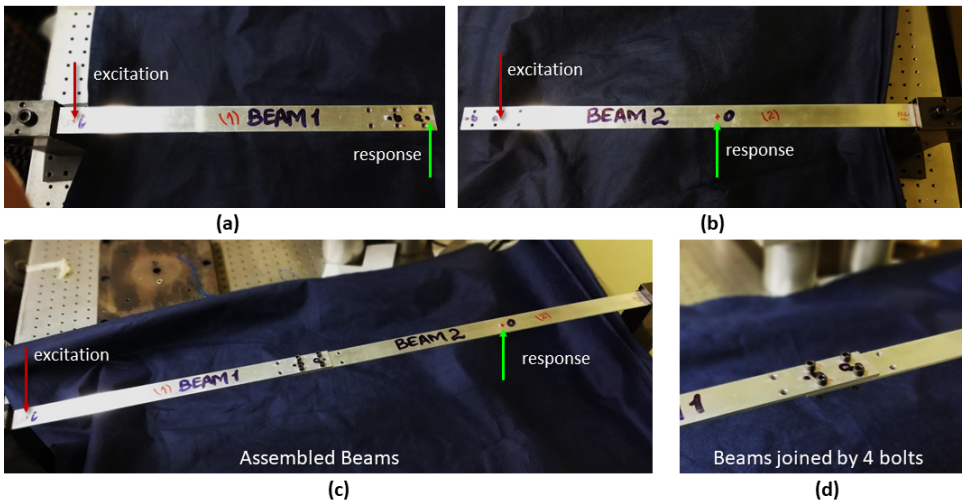

Figure 2. The experimental configuration of the first test-case. (a) Beam-1 (b) beam-2 (both fixed-free) (c) the coupled beams (d) the joint consisting of 4 bolts. The input and response nodes are also shown in the respective figures. The FRFs obtained on these nodes are subsequently used for FE model updating.

Table 1. Test-case 1 Properties.

Properties	Beam1	Beam2
Material	Aluminum	Aluminum
Young's Modulus (GPa)	67	70
Density (kg/m^3)	2400	2600
Dimensions in mm ($L \times W \times H$)	$428 \times 30 \times 3.5$	$572 \times 30 \times 3.5$
Damping coefficient α	2.14	1.21×10^{-7}
Damping coefficient β	1.66	4.20×10^{-7}
	Assembly	
Number of bolts	4	
Bolt material	Steel	

The beams are then modelled in the finite element software, ANSYS APDL v17.2 with actual geometric and updated material properties as listed in Table 1. The meshing is done with SOLID186 brick element with mid-side nodes. Likewise experiments, the bolts are mounted on beam-1 as elastic masses i.e. the density is varied to obtain the required mass. The proportional damping parameters α and β are estimated by modal damping from the measured FRFs [25] and input in the numerical model. The numerical FRFs, thus obtained by modal superposition method are shown for beam 1 and 2 in Fig.3 as green solid lines. During the model updating, attention has been given to the fact that the numerical FRF compares well with the overall experimental FRF, and not just at the natural frequencies i.e. by matching non-resonance and anti-resonance regions in the best possible way [19]. One of the main difficulties in experimental FBS is noise in the signal [12, 15, 17], which is mostly present in the non-resonance regions. Thus the resulting FBS coupling produces fictitious results. This was shown by artificially adding numerical random noise in [15, 17] and will also be shown in this paper for numerical substructuring in the following section, if enough number of modes are not included. Therefore, a compromise on some of the resonance peaks matching is made in the model updating of beam-1 and beam-2. For instance, the third resonance peak in Fig.3(a) and the fourth in Fig.3(b) are off by 4.7% and 3.5%, respectively. A further tuning of FE parameters would have led to shifting of anti-resonances.

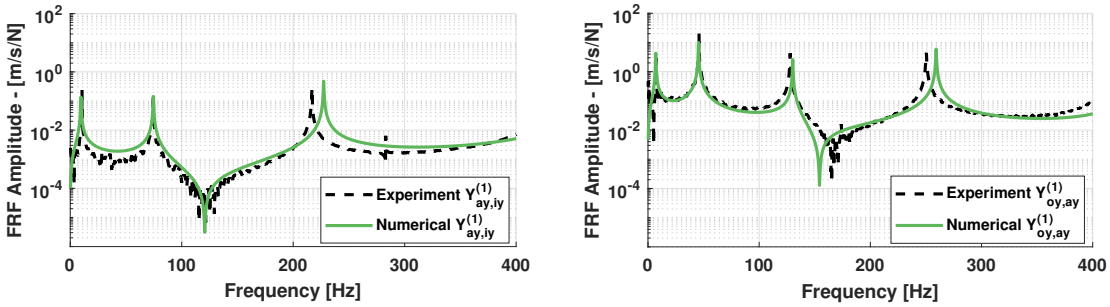

(a) FRFs of Beam 1 (b) FRFs of Beam 2

Figure 3. FRFs of the Beam-1 and Beam-2: FE model updated with the experiment

3.1. Coupling the Beams

The beams are coupled by the LM-FBS method by applying displacement compatibility B at different interface DoFs and reading the desired FRF from the matrix in Eq.5. The FRF corresponding to response at o on beam-2 excited at i on beam-1 (as per Fig.1 and 2), denoted by $Y^{(FBS)}_{oy,iy}$ is shown in Fig.4 for three different interface configurations along with the measured FRF $Y^{(C)}_{oy,iy}$ in y-direction. The first case of 1-interface DoF has not captured the coupled structure's FRF correctly. This is called as ball-joint type behaviour of the interface in [26]. As soon as a second interface DoF is included, the response improves significantly with a very slight improvement by adding the third interface DoF. By adding more interface DoFs, the solution approaches the numerical FRF coupled at all the interface DoFs.

Relative error in frequency shifting of the resonance peaks for the coupled beams' FRFs of Fig.4 is recorded in Table 2. Except for mode 5, the error for 3-DOF interface decreases. This is because beam-1's third mode at 227 Hz and the coupled structure's 5th mode at 233 Hz are quite close i.e. beam-1's behaviour is dominant in determining the coupled system's resonance. The frequency shifts listed in Table 2 are inevitable when considering a few number of discrete interface points. Neverthless, attempts should be made to make them as small as possible. The

amplitude of the reconstructed coupled FRFs is higher, in general. This can be attributed to the fact that the damping estimation at the substructure level is done for each beam constrained at one end.

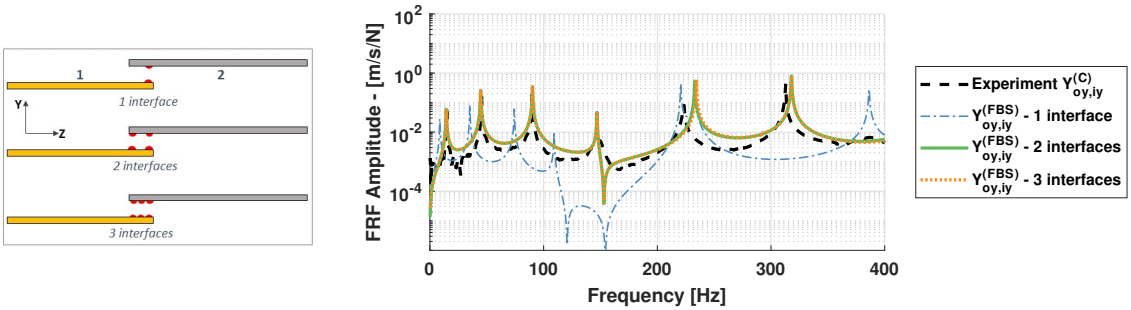

Figure 4. FRFs for the coupled system by using LM-FBS for different interfaces (shown on the left) and compared with the coupled experimental FRF.

The fourth resonance peak of the experimental FRF (black dotted line in Fig.4) shows some non-linear behavior. The FRF decoupling method is helpful here in identifying such characteristics. By looking at the identified interface stiffness k_{11} and damping c_{11} in Fig.5 in the same frequency region, the values are significantly high and confined to the resonance region of the coupled structure. The parameters have been calculated from Eq.6 with a real and imaginary part defined in Eq.7 for 2-interface DoF case. Other terms of Z^*_{int} have a similar pattern but with varying amplitude. The variability in c_{11} at lower frequency comes from noise in the experimental data indicating that the numerical FRF of the coupled system needs to be damped to match exactly the measured FRF.

Table 2. Relative error in modal frequencies of the coupled beams by LM-FBS

Mode #	2 interfaces	3 interfaces
Mode 1	-3.9%	-3.9%
Mode 2	-2.2%	-1.7%
Mode 3	0.2%	0.2%
Mode 4	-0.7%	-0.6%
Mode 5	4.4%	4.8%
Mode 6	1.6%	1.6%

3.2. Discussion on Test-case 1 Results

The results shown above as well as the literature present some important findings before proceeding to the next test-case. In order to reconstruct a coupled system response solely from experimental FRFs, the LM-FBS in its classical form and without any filtration or data-processing is very difficult [17, 19]. By using multiple interface translational DoFs, the identification yields better results [21]. In order to capture other dynamic modes especially at higher frequencies, translational DoFs in other directions are also necessary. However, it quickly increases the size of the problem and makes it practically difficult to perform FRF

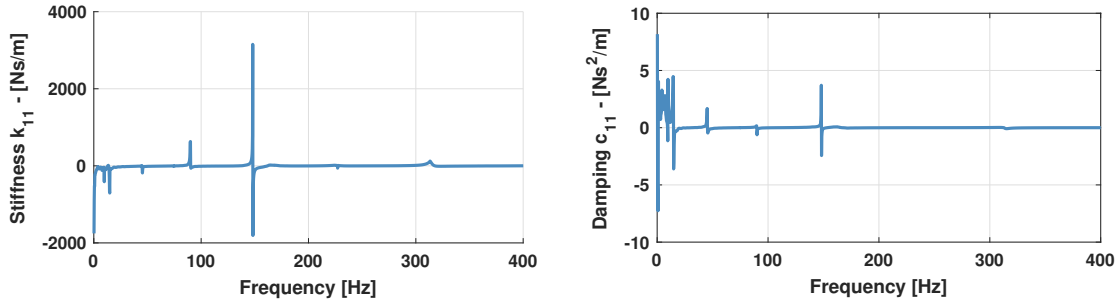

(a) Interface Stiffness (b) Interface Damping

Figure 5. Interface Stiffness k_{mn} and Damping c_{mn} of the 2-interface DoF case for $m = n = 1$.

measurements at multiple discrete points and in different directions. The drive point FRFs on a slender structure like the beams in this study are even harder to be obtained. This may necessitate hybrid approaches where one substructure's FRFs can be obtained numerically yet it requires that the FRFs on the other substructure are measured. In the case, when the substructures have complex and twisted geometries such as the bladed-disk discussed in the next section, direct FRF measurement at the interface is very difficult due to narrow spaces in the root-joint. Therefore, the suggested method of FE model updating FRFs for some accessible DoFs, and then the extraction of numerical FRFs at the remaining DoFs can be a convenient way of substructuring and interface identification.

4. Test-Case 2 - The Bladed-disk

The second test-case for this study is the bladed-disk assembly with 18 blades inserted in the disk slots, as shown in top-left of Fig.6. In this study, only one blade at a time is coupled with the disk and examined for the LM-FBS coupling, also depicted in the figure. The disk as a stand-alone substructure is constrained at the center whereas the blade is not constrained. In this way, all the interfaces or root-joints on the assembly can be dynamically characterized and the damping variability or contact mistuning can be identified for the bladed-disk system. Both the disk and the blade in this study are made of Steel with Young's modulus $E = 206GPa$ and density $\rho = 7800kg/m^3$.

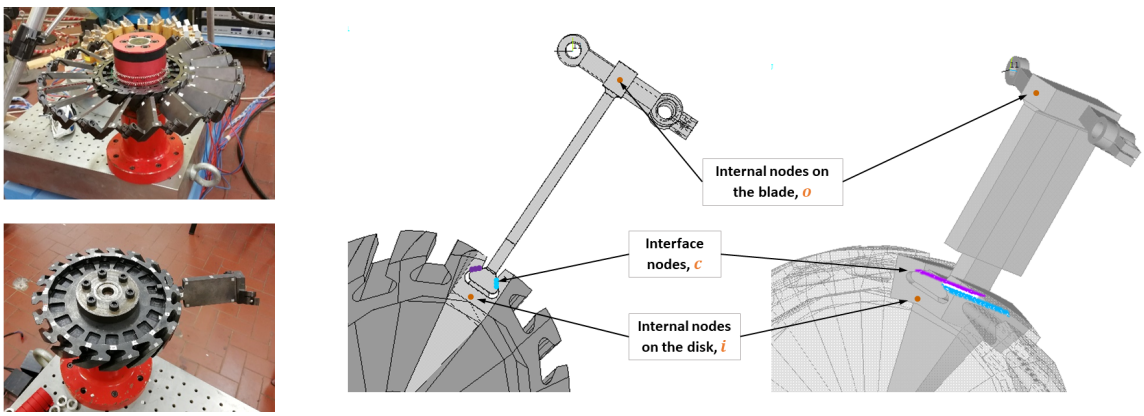

Figure 6. The bladed-disk with 18 blades assembled (top-left), the disk with only one blade (bottom-left) and the model (on the right) of the blade-disk showing locations of the input, response and interface nodes.

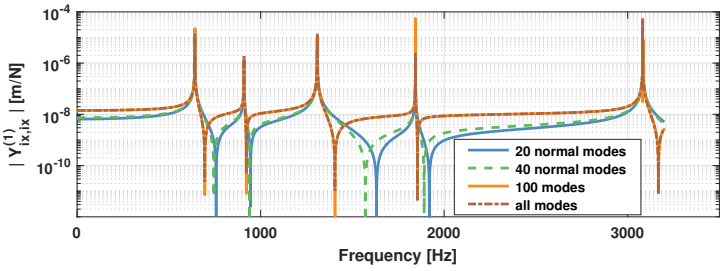

Figure 7. Effect of normal modes on drive point FRF $Y^{(1)}_{ix,ix}$ of substructure 1 (disk).

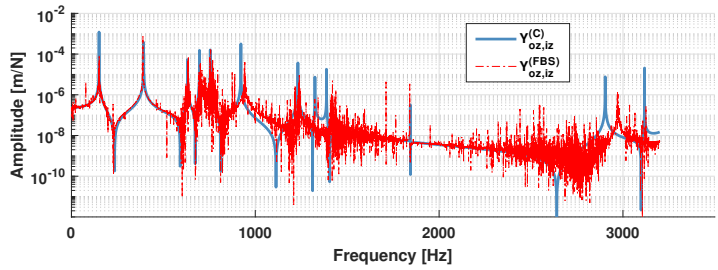

Figure 8. Effect of low number of normal modes on the reconstructed FRF $Y^{(FBS)}_{oz,iz}$ of the coupled structure. Number of normal modes = 20.

It is evident from the geometry that more DoFs per interface node will be needed for accurate response but due to the narrow space at the joint, a complete measurement-based FRF campaign is not possible in terms of both the response measurement and the excitation direction. Presence of high modal density region can also induce additional problems. For a subsequent non-linear analysis, defining contact elements at all the interface nodes will not be an economical option. Therefore, by taking advantage of the decoupling method, a sensitivity analysis is performed on the model shown in Fig.6 where the necessary nodes have been labeled. The model is discretized using Solid brick elements like the first test-case. Since the method requires a full disk computational model instead of a sector, a model order reduction was done according to Eq.8 with 40 fixed interface modes $\phi^{(s)}$. Including more fixed interface modes did not have a signficant difference. The natural frequency variation of the reduced system was less than 0.5% for the modes in the frequency band of 0-3200 Hz. Thus, the final size of the problem became 1516 DoFs including all the interface DoFs $u_c^{(s)}$, 6 internal DoFs $u_i^{(s)}$ and 40 fixed interface modal amplitudes $q^{(s)}$ for each substructure. In the reduced model, modal superposition method was used to avoid the matrix inversion. The FRFs obtained by keeping different number of normal modes in modal superposition method revealed some interesting findings. Fig.7 shows drive point FRF of the disk substructure constructed by different normal modes. The solution required high number of modes at least up to 100 for the non-resonance response. This seems due to high modal density of the disk whereas for the blade, the solution did not require as many modes. If the substructure FRFs are generated with 20 normal modes, then the reconstructed coupled response in Fig.8 looks very noisy. The response is captured well around the resonances but the remainder part has a lot of spurious peaks. This re-emphasizes one of the findings discussed in Section 3 regarding modelling of the substructure FRFs not only at the resonances but also at the non-resonance regions.

By consecutively including one, two, three and four number of nodes per side of the interface (i.e. there are two sides of the interface and 3 DoFs per node are used), the FRFs reconstructed for the coupled system using the LM-FBS method are shown in Fig.9. The interface nodes are also shown to the left of each sub-figure. A comparison is made with the FRF of the coupling by fully merged interface i.e. by applying the displacement compatibility at all the interface DoFs.

As expected, the results improve by successively increasing the number of nodes or DoFs. By merely considering 4 interface nodes (12 DoFs) out of a total of 245 nodes per side, a considerably

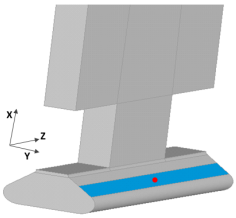

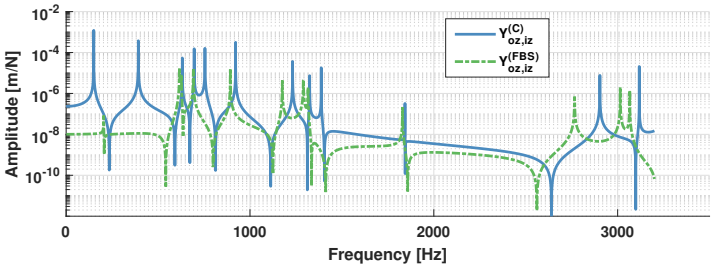

(a) for 1 interface node per side

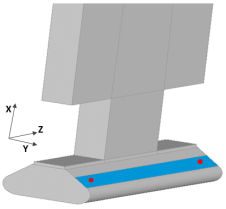

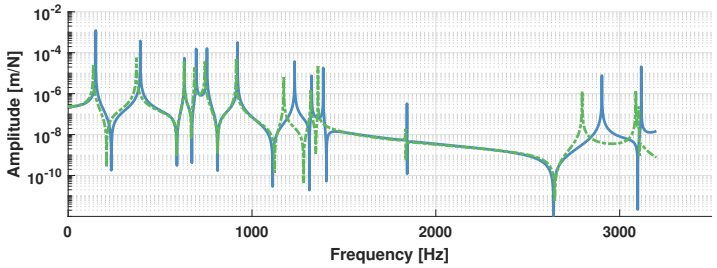

(b) for 2 interface nodes per side

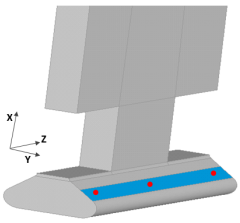

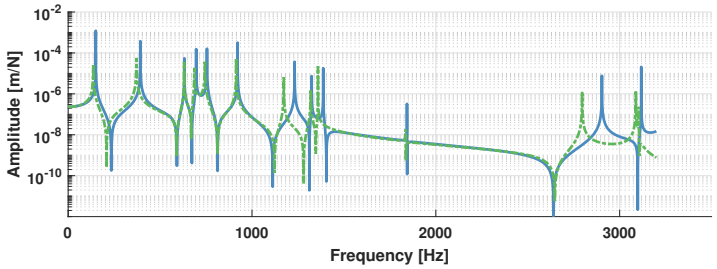

(c) for 3 interface nodes per side

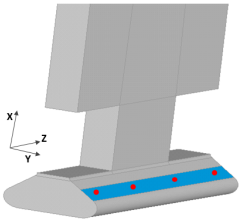

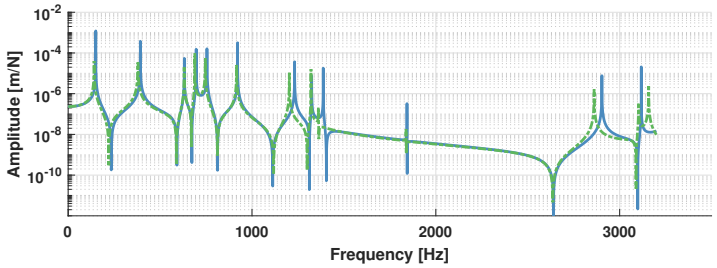

(d) for 4 interface nodes per side

Figure 9. FRFs obtained by the LM-FBS method on the bladed-disk by considering different nodes per side. Each node is described by 3 DoFs. —— numerical FRF of the coupled structure, – – – FRF obtained by LM-FBS.

good agreement is found up to at 1200 Hz. Since the damping is not included, differences in the amplitude peaks at resonances are ignored. The first high modal density region between 600 Hz to 760 Hz is very well approximated even with just two interface nodes per side. It is further seen quantitatively in Fig.10 and Table 3 that mode 3, 4 and 5 have a small error of less than 2% with just 2 nodes per side. This implies that the choice of nodes gives nearly rigid behavior of the interface for these frequencies. The second high modal density region between 1200 Hz to 1400 Hz is not captured well by 4 nodes per side. The high frequency region, of course, would need more DoFs for a better reconstruction. The choice of number of interface nodes depends on the modes of interest. If the modes of interest are reasonably approximated by using limited

Table 3. Relative Error in Natural Frequencies of the coupled blade and disk by LM-FBS.

Nodes per side	Mode1	Mode2	Mode3	Mode4	Mode5
1	15.9%	55.4%	-2.4%	-3.7%	17.7%
2	-8.8%	-5.2%	-0.2%	-1.4%	-1.5%
3	-6.1%	-3.4%	-0.2%	-1.1%	-1.2%
4	-4.5%	-2.7%	-0.2%	-0.8%	1.1%
5	-4.1%	-2.2%	-0.2%	-0.6%	-0.8%

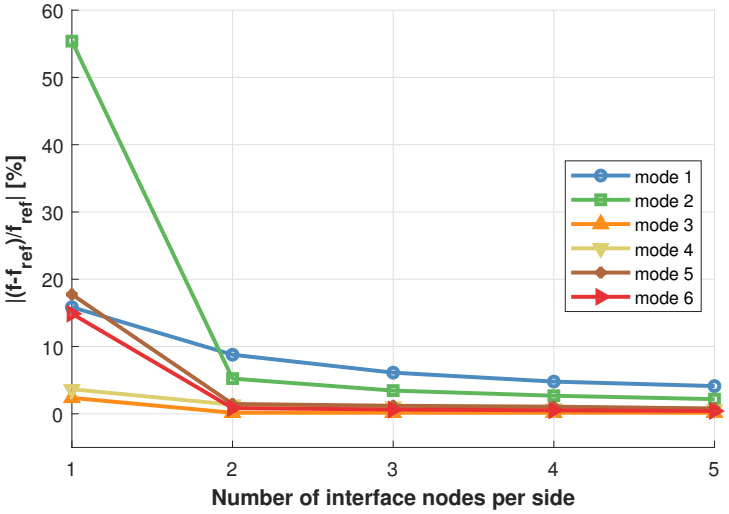

Figure 10. Absolute relative error in modal frequencies as a function of number of interface nodes. f_{ref} is the reference frequency from the fully merged interface.

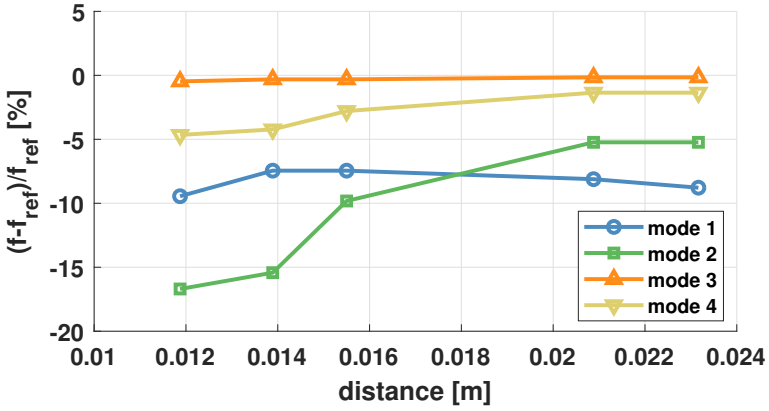

Figure 11. Relative error in modal frequencies for 2-interface nodes per side as a function of distance between the nodes. f_{ref} is the reference frequency from the fully merged interface.

number of DoFs, then these DoFs with an approximately identified contact parameter can be used for onward non-linear analysis.

For the case of 2-nodes interface of Fig.9(b), a further sensitivity is done against the distance between the two nodes which is presented in Fig.11. The relative error is high if the two nodes are closely spaced. It starts decreasing as the distance increases, however, an increasing trend can be noticed if the nodes are placed at the edges especially for the first mode. The FRF shown earlier in Fig.9(b) corresponded to the location that had the lowest error.

5. Conclusions

In this paper, the Lagrange multiplier frequency based method has been applied to two different test cases of substructures. A first simple test case with two beams and a second one of more complex geometry with a disk coupled to one blade.

For the first test-case of two cantilevered beams, the FRFs are measured separately for each beam at only a few interface DoFs (out-of-plane defections). The numerical models of the two separate beams (substructures) are updated to match the corresponding measured FRFs. The two updated numerical substructures are then coupled by means of the LM-FBS technique for different number of interface DoFs. The resulting coupling FRFs match well with the measured FRFs of the assembled structure, but the agreement improves by increasing the number of interface DoFs. This proves that, even for a simple structure with two beams, the requirement of several interface DoFs makes very onerous to obtain all the FRFs experimentally. On the contrary the applied hybrid approach, where the FRFs of the single structures are computed numerically and updated against the corresponding experimental ones, proved to be very convenient since it allows to choose the desired number of interface DoFs.

It was also shown that for a resonance peak, showing a shape typical of non linear behaviour, the technique of the FRF decoupling can be applied to identify interface parameters.

For the more complex geometry of the second test-case (disk and blade), the numerical FRF reconstruction was adopted. Due to the huge size of the FE models an initial Craig-Bampton reduction was deemed necessary both for the FE model of the disk and the blade (substructures) retaining all the interface DoFs. The FRFs were computed for each substructure by using modal superposition method. It was demonstrated that in the modal superposition method the number of the chosen normal modes is important in order to obtain, for each substructure, an accurate FRF not only at the resonances but also at the non-resonance regions. This accuracy of the FRF of each substructure is a necessary starting condition to obtain a good reconstructed FRF of the full structure by the LM-FBS technique. A sensitivity analysis was then performed by applying the LM-FBS technique to reconstruct the FRF of the full structure (disk and blade) using a different number of interface DoFs. It was proved that the needed number of interface nodes (i.e. interface DoFs) depends on the frequency range of interest. In this case for the reconstruction of the full system response for first five modes (in the range 600-760Hz) keeping 4-5 nodes at each interface of the blade root can be considered enough.

Once the number of required interface nodes are settled, the FRF decoupling technique will be employed to identify for the disk-blade the interface parameters. This procedure will be repeated for each blade of the disk. The final aim is to establish a method for the reconstruction, in a given frequency range, of the FRFs of the bladed disk with all the blades.

Acknowledgements

This work is a part of the project EXPERTISE funded by the European Union's H2020 research and innovation program under the Marie Sklodowska-Curie grant agreement No. 721865.

References

[1] Thomas D L 1979 *International Journal for Numerical Methods in Engineering* **14** 81–102
[2] Castanier M and Pierre C 2006 *Journal of Propulsion and Power* **22** 384–396 ISSN 0748-4658 URL `http://doi.aiaa.org/10.2514/1.16345`
[3] Bladh J R 2001 *Efficient Predictions of the Vibratory Response of Mistuned Bladed Disks By Reduced Order Modeling* Ph.D. thesis University of Michigan
[4] Vargiu P, Firrone C M, Zucca S and Gola M M 2011 *International Journal of Mechanical Sciences* ISSN 00207403
[5] Castanier M P and Pierre C 2002 *AIAA Journal* ISSN 0001-1452
[6] Beirow B, Giersch T, Kühhorn A and Nipkau J 2014 *Journal of Engineering for Gas Turbines and Power* ISSN 0742-4795

[7] Seinturier E, Lombard J P, Dumas M, Dupont C, Sharma V and Dupeux J 2004 *Proceedings of ASME Turbo Expo 2004* 317–326
[8] Salles L, Blanc L, Thouverez F, Gouskov A M and Jean P 2009 *Volume 6: Structures and Dynamics, Parts A and B* 465–476 ISSN 20952686 URL http://proceedings.asmedigitalcollection.asme.org/proceeding.aspx?articleid=1647364
[9] Firrone C M and Zucca S 2011 *Numerical Analysis - Theory and Application* 301–334 ISSN 1089-5639, 1520-5215 URL
[10] Yumer M E, Cigeroglu E and Özgüven H N 2013 *Journal of Turbomachinery* **135** 031008 ISSN 0889-504X URL http://turbomachinery.asmedigitalcollection.asme.org/article.aspx?doi=10.1115/1.4006667
[11] Zucca S 2017 *Nonlinear Dynamics* **87** 2445–2455 ISSN 1573269X
[12] de Klerk D, Rixen D J and Voormeeren S N 2008 *AIAA Journal* **46** 1169–1181 ISSN 0001-1452 URL http://arc.aiaa.org/doi/10.2514/1.33274
[13] Tsai J S and Chou Y F 1988 *Journal of Sound and Vibration* **125** 487–502 ISSN 10958568
[14] Rixen D J 2008 How measurement inaccuracies induce spurious peaks in frequency based substructuring *IMAC XXVI - International Modal Analysis Conference* ISBN 0-912053-98-4 ISSN 21915644
[15] D'Ambrogio W and Fregolent A 2016 *Mechanical Systems and Signal Processing* ISSN 10961216
[16] Mayes R, Rixen D, Allen M and Dynamics S 2013 *Sem: Imac Xxxi* **2** 331
[17] Drozg A, Čepon G and Boltežar M 2018 *Mechanical Systems and Signal Processing* **98** 570–579 ISSN 10961216
[18] Duarte M L M and Ewins D J 2000 *Mechanical Systems and Signal Processing* **14** 205–227 ISSN 08883270
[19] Pagnacco E, Gautrelet C, Paumelle J, Lambert S and Rixen D J 2009 *20th International Congress of Mechanical Engineering*
[20] Pasma E A, Seijs M V V D, Klaassen S W B and Kooij M W V D 2018 *Conference Proceedings of the IMAC18* 0–7
[21] Tol and Özgüven H N 2015 *Mechanical Systems and Signal Processing* ISSN 10961216
[22] de Klerk D, Rixen D J and de Jong J 2006 *24th international modal analysis ...* ISSN 21915644
[23] Kalaycoğlu T and Özgüven H N 2018 *Mechanical Systems and Signal Processing* **102** 230–244 ISSN 10961216
[24] BAMPTON M C C and CRAIG JR R R 1968 *AIAA Journal* ISSN 0001-1452
[25] Richardson M and Schwarz B 2003 *Sound And Vibration* **37** 1–8 ISSN 15410161 URL http://www.sandvmag.com/downloads/0301rich.pdf
[26] Haeussler M, Sendlbeck S and Rixen D 2018 Automated Correction of Sensor Orientation in Experimental Dynamic Substructuring *Dynamics of Coupled Structures, Volume 4.* (Springer) pp 65–70